Acta Materialia 105 (2016) 147–154

Contents lists available at ScienceDirect

Acta Materialia

journal homepage: www.elsevier.com/locate/actamat

Full length article

Interstitial emission at grain boundary in nanolayered alpha-Fe

Xiao-Zhi Tang [a], Ya-Fang Guo [a, *], Yue Fan [b], Sidney Yip [c], Bilge Yildiz [c, **]

[a] Institute of Engineering Mechanics, Beijing Jiaotong University, Beijing 100044, China
[b] Materials Science and Technology Division, Oak Ridge National Laboratory, Oak Ridge, TN 37831, USA
[c] Department of Nuclear Science and Engineering, Massachusetts Institute of Technology, 77 Massachusetts Avenue, Cambridge, MA 02139, USA

ARTICLE INFO

Article history:
Received 25 August 2015
Received in revised form
3 December 2015
Accepted 4 December 2015
Available online 24 December 2015

Keywords:
Defect annihilation
Grain boundary
Potential energy landscape
Rate theory

ABSTRACT

The Autonomous Basin Climbing method and Rate Theory are applied to investigate the interstitial emission mechanism in alpha-Fe. The atomic trajectories and potential energy landscape of the interstitial emission process induced by the Σ3<110>{111} symmetrical tilt grain boundary are presented. By comparing with vacancy hopping mechanism, the grain boundary influence range at finite temperature is revealed. We uncover the energetic and geometric essentials of the interstitial emission mechanism, and find connections between two previously reported defect-grain boundary interactions at long time scale. Surprisingly in nanolayered structures, higher grain boundary density raises the activation energy barriers of interstitial emission. This phenomenon is strongly correlated with the energy and local stress distribution of the grain boundary.

1. Introduction

Stainless steels are widely used in the core structure of fission reactors where materials are exposed to severe irradiation environments [1–3]. After collision cascades, those interstitials and vacancies which escaped the dynamic annealing process degrade material properties by the formation of extended defects [4,5]. Therefore structure-engineered materials, such as nanograined or nanolayered metals which offers better self-healing mechanisms, have been a subject of great interest [6,7]. The enhanced tolerance of radiation-induced point defects of these materials comes from higher grain boundary (GB) density.

GBs are known to be effective biased sinks for interstitials over vacancies [8], and, at long time scale, it has a surprising "loading-unloading" effect. Upon irradiation, self-interstitial atoms (SIAs) are loaded into the boundary, and then, emitted to annihilate immobile vacancies in the bulk [9]. This emission-induced recombination was first studied in fcc Cu in 2010 by applying Temperature Accelerated Dynamics (TAD) in simulations at 300 K [9]. Atomic scale details within hundreds of nanoseconds revealed the kinetic behavior and spatial character of this so-called "interstitial emission" mechanism. In 2012, boundary-defect interactions in alpha-Fe at 450 K [10] were revealed to be mediated by formation and annealing of chain-like defects, which consist of alternately positioned interstitials and vacancies. Two kinds of chain defects were identified in that study, "bulk chain-like" (BC) defect and "grain boundary chain-like" (GBC) defect. The boundary-defect interaction occurred within less than several nanoseconds, while with a higher energy barrier than that for SIA emission in Cu.

In this work, we focus on the investigation of emission-induced recombination mechanism between a vacancy and an interstitial atom at long time scale in alpha-Fe. The autonomous basin climbing (ABC) method [11] along with rate theory (RT) [12] are used in our study. The Σ3<110>{111} symmetrical tilt grain boundary (STGB), a widely studied representative interface on which the mechanical properties are strongly dependent on, is used as our modeling system. Additionally, a nanolayered alpha-Fe model containing four Σ3<110>{111} GBs is also formulated to investigate the influence of GB density on the energy barrier of both SIA emission and vacancy hopping.

2. Simulation procedure

Two modeling systems are established, the one-GB model and the nanolayered structure model, where a single self-interstitial atom is loaded into the GB and a vacancy is placed nearby. Fig. 1(a) is the one-GB model which contains a Σ3<110>{111} STGB with the tilt axis of $[\bar{1}10]$. The crystallographic orientation of grain 1 is shown in the figure. The simulation system of the one-GB model

* Corresponding author.
** Corresponding author.
E-mail addresses: yfguo@bjtu.edu.cn (Y.-F. Guo), byildiz@mit.edu (B. Yildiz).

http://dx.doi.org/10.1016/j.actamat.2015.12.009
1359-6454/

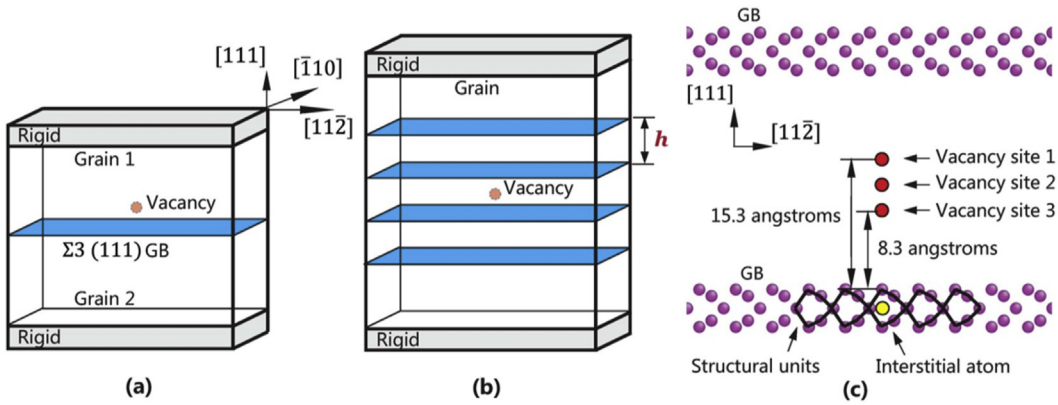

Fig. 1. Schematic of simulation systems. (a) One-GB model. (b) Nanolayered structure model. (c) Σ3<110>{111} GB structure in alpha-Fe and positions of the vacancy and the interstitial atom.

is approximately 140*130*16 Å in three dimensions, containing around 3×10^5 atoms. Fig. 1(b) is the nanolayered structure model containing four parallel Σ3<110>{111} STGBs. The simulation system of this nanolayered structure model is slightly larger in [111] direction, and the distance between each GB is about 20 Å, indicated as *h* in Fig. 1(b). For both models, periodic boundary conditions (PBCs) are applied in [11$\bar{2}$] and [1$\bar{1}$0], parallel to the GB plane, and the relative positions of rigid regions are kept constant.

Fig. 1(c) shows the Σ3<110>{111} GB structure in alpha-Fe and the positions of the vacancy and the interstitial atom in our simulation. To construct aΣ3<110>{111} GB in our model, atoms in the contact region of two grains within a specified cutoff distance of separation are deleted. Then a rigid-body translation in all three Cartesian directions is applied to determine the stable structure, followed by a steepest decent energy minimization of all the free atoms to get the lowest grain boundary energy. The basic geometric and energetic parameters of the Σ3<110>{111} GB are summarized in Table 1, using Finnis and Sinclair EAM potential developed by Ackland et al. [13]. It is seen that the excess free volume in our model is larger than that in Refs. [14] and [15]. Two reasons can be given for this discrepancy. First different methods were used, DFT in Refs. [14] and [15] and molecular statics (MS) simulation in our calculation. Secondly, in Refs. [15], parallel GBs are placed at distance less than 10 Å. The local stress distribution makes them attractive to each other, so the relaxed equilibrium structure should have smaller volume than obtained by MS simulation.

As Ref. [15] pointed out, <110> STGBs in bcc metals can be interpreted by the "structural unit" [16] model. The structural units in our modeling system are outlined by the solid black lines in Fig. 1(c). These structural units enhance interface diffusion by their inherent local free volume [17]. Previously, similar interface diffusion mechanism was found in Cu [18,19], suggesting that structural units are ideal interstitial sites. To load an originally pristine GB with one interstitial in our modeling systems, we have used two methods, MS simulation and ABC method. In the MS simulation, the SIA was placed in the "spontaneous annihilation region" [20] near the GB, and then through an energy minimization of the whole system the SIA was absorbed by the GB. In the ABC method, the SIA was placed at an octahedral site near the GB. The system was activated to climb out of its existing energy minimum, to settle into a final state in which the interstitial moved into the structural unit of the GB. Both methods gave the same configuration of interstitial-loaded GB shown in Fig. 1(c). Similar to the result in Cu [18,19], the SIA location is at the center of structural unit.

Table 1
Basic GB properties.

Reference	Misorientation (°)	GB energy (mJ/m^2)	Excess free volume (Å)
This work	109	1380	0.80
Ref. [30]	109.47	1308	
Ref. [14]	109.47	1200	0.31*
Ref. [21]	~110	~1300	
Ref. [15]		1610*	0.31*

* Result by first-principle calculations.

Another part of building our modeling system for the interstitial emission simulation is to place a vacancy in the vicinity of the GB. Three vacancy sites along the <111> close-packed direction are chosen, denoted as site 1, 2 and 3, as shown in Fig. 1(c). Both the vacancy and the interstitial are on the same [111] lattice line. The distance of these vacancy sites to the GB is 15.3 Å, 11.8 Å, and 8.3 Å, separately. Geometrically site 2 is in the middle of the other two sites. The selection of these three sites is based on the following considerations. For a pristine GB, a previous work [21] chose a distance range of 15 Å from the GB to investigate the vacancy absorption. They found that the binding energy of vacancy decreases to nearly zero when it is placed more than 10 Å away from the <110> STGB in Fe. So considering the indicated length scale in Ref. [21], it is reasonable to take 15 Å as the maximum distance in our simulation. For an interstitial-rich GB, the influence region is recently defined as a range of 5–10 Å (on each side) upon the analysis on both the energetic and kinetic behavior of point defects nearby [20]. Although this definition came from the case of <100> STGB in Fe, it is a reasonable reference for our simulation. For GB-induced annihilation mechanism itself, as stated by Ref. [10], it may not occur if two defects are separated too far apart, because such removal mechanism is stress-field induced. In Ref. [10] and Ref. [9] which reported the defect annihilation mechanism, the defects were only approximately 10 Å away from the GB. These three vacancy sites are chosen in our simulation with these considerations in mind as we probe the phenomenon of defect annihilation and compare it with the conventional vacancy hopping mechanism.

For the nanolayered structure model, it is important to decide the layer thickness, referring to the spacing *h* between parallel GBs in Fig. 1(b). In 2004, Heinisch et al. [22] selected a 60-Å-spaced Cu–Ni interface in their simulation of displacement cascade. Three years later, experimental results on 25 Å Cu–Nb multilayer composites were reported in a radiation damage study [23]. In 2008,

Demkowics et al. used Cu–Nb bilayer as their simulation model, where interfaces are spaced at 20 Å [24]. In the same year, TEM observation of a sputter-deposited 10 Å Cu–Nb nanolayered composite was reported [6]. Recently in 2010, 10 Å thick nanolayer film was synthesized on HF etched Si substrates [25]. Although nanolayered single-element Fe was not popular due to technical difficulty or low industrial need for now, the reduction in interface spacing does indicate interests in thinner layer down to 10 Å. Thus in this work, STGBs are 20 Å away from each other, making vacancy site 2 in the right middle of the two interfaces, as Fig. 1(b) shows.

All the present simulations were performed using LAMMPS [26] with the ABC algorithm implemented as a user package. The ABC algorithm was developed by Kushima et al. [11] as an atomistic activation-relaxation technique for sampling transition-state pathways. It is proved to be highly efficient on sampling and reconstructing the system's potential energy surface (PES). In alpha-Fe, it has been applied for studying the unfaulting of self-trapped SIA clusters [27], void nucleation [28], and thermal creep [29]. Starting with a minimum-energy configuration with N atoms, ABC method adds Gaussian penalty functions to the potential energy of the entire 3N-dimensional space, and pushes the system away from the initial configuration, until it enters into an adjacent potential energy well. Therefore, ABC method can be useful in finding reaction paths and low-probability final configurations without knowing them in advance.

3. Results and discussion

3.1. Interstitial emission pathway on potential energy landscape

In this section, the energy landscape for SIA emission is found by the ABC method. The atomistic configuration C1 in Fig. 1(c) is the initial state, where the vacancy is located on site 2. Then, the system was activated by energy penalty functions, and pushed into a series of energy minima indicated as C2 to C4 in Fig. 2(a), which represent the minimum-energy configurations for the SIA emission process. In Fig. 2(b), nudged elastic band (NEB) method was employed between these configurations, for a better description of PES and getting more accurate barriers. It is found in Fig. 2(b) that the SIA emission reduces system energy by 1.71 eV, and both C2 and C3 configurations are metastable due to their small barriers (<0.2 eV). More importantly, 0.9 eV is found to be the barrier of SIA emission, which will be the topic in the next section. Depicting the four minimum-energy configurations in sequence, Fig. 2(c) shows in detail how the GB emits an interstitial atom to annihilate a vacancy located nearby. Initially in C1, due to the absorbed SIA, atoms around it which belong to the structural unit are slightly pushed away from its original lattice sites, leading to a higher energy state of atoms along [111] direction. Once the SIA is emitted, the excess energy at GB is released and the vacancy is absorbed through the two intermediate states (C2 and C3). As shown in C4, the GB recovers its pristine configuration after this interstitial emission process. It is worth noting that all the emission mechanisms found in this work can be described appropriately by this process.

3.2. Energy barriers of vacancy diffusion and interstitial emission

Fig. 3 lists separately the barriers of vacancy hop and SIA emission for the three vacancy sites in the One-GB model by NEB calculations. Among them, site 1 is the farthest from the GB, therefore as can be seen in Fig. 3(a), the vacancy hop barrier at this site is nearly the same as the value in the bulk, 0.63 eV [13]. While site 2 is 11.8 Å away from the GB, within the GB influence range, and we find a slight reduction on diffusion barrier of 0.04 eV compared to site 1. This observation is consistent with the statement in Ref. [21] that the diffusion barrier of the vacancy gradually decreases as it approaches the GB, even though in this work the GB is SIA-loaded, not pristine. At site 3, the vacancy is only 8.3 Å to the GB, and the diffusion barrier significantly increases to 0.90 eV. Besides, the energy of final sate of the vacancy hop on site 3 is higher than the initial state by 0.22 eV, indicating that the vacancy prefers to stay at site 3, instead of diffusing towards the SIA-loaded GB.

In contrast to the hopping mechanism, the SIA emission barrier which dominates the state transition from C1 to C2 is significantly reduced as the vacancy approaches the GB as shown in Fig. 3(b).

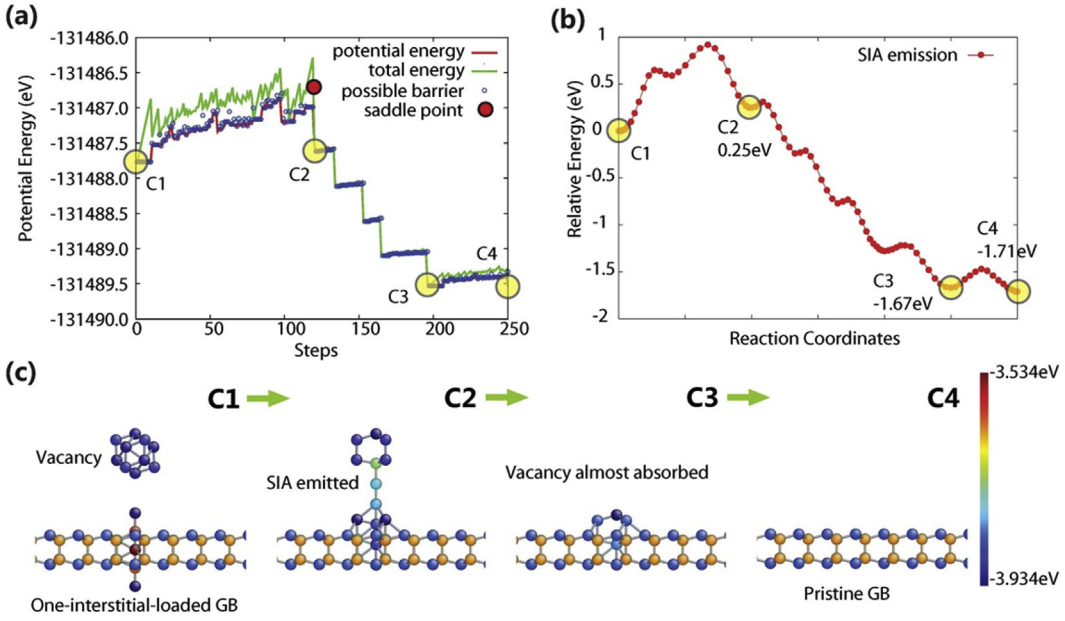

Fig. 2. (a) Evolution of energy as derived by the ABC method. (b) The potential energy landscape associated with the atomic configurations described in (c). (c) Atomic trajectories of SIA emission. Atoms with energy lower than −3.934 eV are not shown. Visualized by AtomEye [31].

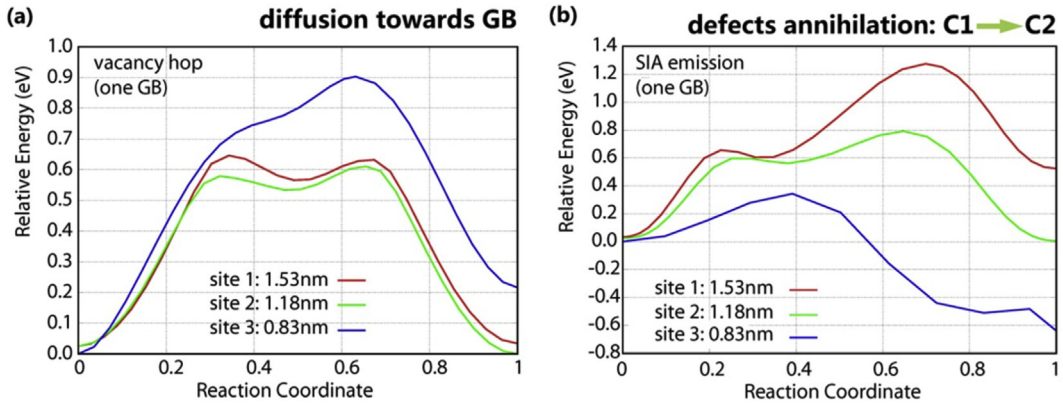

Fig. 3. Energy barriers of (a) vacancy hop and (b) SIA emission for three selected vacancy sites (only for one-GB model), obtained by NEB calculations.

Particularly on site 3, the SIA emission barrier is only 0.34 eV, much smaller than the hopping barrier of 0.90 eV. The same trend of barrier variation on vacancy hopping and SIA emission is also found in nanolayered structure system shown in Fig. 4. It means during the defect absorption process, when a vacancy is located on site 3, the SIA emission mechanism is relatively easier to be activated at any temperature, while the hopping mechanism is not preferred since it does not lower the system potential energy. The corresponding activation temperature for emission mechanism is shown in Table 2 given by rate theory (RT), defined by a transition time of 1 s. The time is calculated by

$$t = k_0^{-1} \times \exp(E_a/k_B T). \quad (1)$$

The attempt frequency k_0 is chosen to be 10^{12} s^{-1}, and E_a is the activation barrier obtained by NEB. k_B and T are Boltzmann constant and temperature respectively.

Based on the analysis above, two results are obtained on how vacancies interact with single-interstitial-loaded GB in alpha-Fe. There is a competitive mechanism between conventional vacancy diffusion and SIA emission, reflected in the variance of energy barriers. On site 3, SIA emission is proved to be more efficient for point-defect recombination because of its smaller energy barrier. On site 1, according to the RT calculation results in Table 2, the activate temperature of the emission mechanism at the rate of one time per second is around 521 K. Therefore at long time scale, SIA emission is still active and efficient at finite temperatures when a vacancy is on site 1, since hopping mechanism with a barrier nearly equals to the bulk value is unable to drive the vacancy towards the GB. The SIA emission mechanism demonstrates its importance in the radiation damage annealing near the GB. Secondly, the dependence of the interaction between vacancy and single-interstitial-loaded GB on their separation distance is revealed, which is different from the previously reported statistical results [21]. For Σ3<110>{111} STGB in our simulation, when the vacancy is close enough (on site 3), the SIA-loaded GB affect the kinetic behavior of vacancies by repelling the hopping mechanism, reflected in the barrier increase. While in conventional knowledge, vacancy diffusion barriers should decrease as the vacancy approaches the interstitial-loaded GB [20]. This discrepancy is supposed to be explained in the following way. Generally speaking, the mean barriers of vacancy diffusion towards the interstitial-loaded GB are reduced as a function of the distance, but there are still some sites giving higher barriers than the bulk value [20]. As Ref. [9] stated, for the interstitial-loaded GB, the vacancy diffusion barriers are quite variable because of the complex strain fields, which might also be the reason for our observation. So it is not a surprise to observe an increase of diffusion barrier in our work when the vacancy approaches the GB, because only three specific sites are considered. Future work will provide more data to find the inherence of this repellence phenomenon, covering all the possible vacancy sites and concerning different materials.

3.3. *Defect absorption length scale and its variation in nanolayered structure*

To investigate the absorption length scale, we analyze the energetic behavior of a vacancy interacting with Σ3<110>{111} GB.

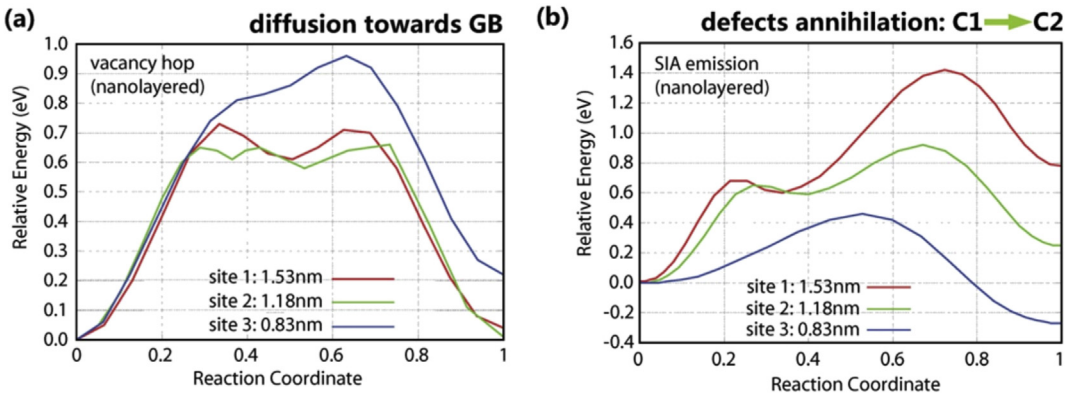

Fig. 4. Energy barriers of (a) vacancy hop and (b) SIA emission at the selected three sites in the nanolayered structure model.

Table 2
Activation temperature of SIA emission.

SIA emission	One-GB			Nanolayered structure		
	Site 1	Site 2	Site 3	Site 1	Site 2	Site 3
Barrier (eV)	1.24	0.77	0.34	1.42	0.92	0.47
Activation temperature (K)	521	323	142	596	386	187

The binding energies of a vacancy in the vicinity of the pristine GB, one-SIA-loaded GB, and nanolayered structure (none of/only one-GB is interstitial-loaded) are calculated and plotted in Fig. 5(a). The binding energy E_b^α is defined as

$$E_b^\alpha = E_f^{bulk} - \left(E_{GB}^\alpha - E_{GB} + E_{coh}\right), \quad (2)$$

where E_{coh} is the cohesive energy per atom (−4.01 eV in this work, while −4.12 eV in Ref. [20], and −4.316 eV in Ref. [13]), E_{GB}^α and E_{GB} are the total energies of the simulation cell with and without the vacancy, E_f^{bulk} is the bulk defect formation energy.

In Fig. 5(a), for a pristine GB, the negative binding energy values on some sites indicate that it is not energetically favorable for a vacancy to locate at those sites. This phenomenon has also been observed in Ref. [21], indicating that Σ3(111) STGB is not among those general GBs which reduce the formation energy of a vacancy nearby. When a SIA is trapped at the GB, all the binding energies are positive due to the potential recombination mechanisms (vacancy hop or SIA emission). Moreover, the nanolayered structure with one-GB SIA-loaded makes binding energies drop again by approximately 0.03 eV, reflecting the density increase of pristine GBs. Apparently, if we remove the SIA trapped in the nanolayered structure, the binding energy would decrease to 0.75 eV, but still positive. This means that pristine Σ3<110>{111} GB is not a vacancy sink. But when it is interstitial-loaded, a vacancy located nearby reduces the system energy by quite small amounts less than 0.3 eV, still making the location of vacancies energetically favorable.

Previous MS calculations in Fe [30] suggested that the vacancy binding energy is correlated with the GB parameter. Therefore, the complex local energy/stress distribution at the structural units, along with the high free volume at the interface, can be used to analyze the negative binding energies correlated with a pristine Σ3<110>{111} GB. As Fig. 5(b) shows, despite the Σ3(111) STGB having a high GB energy of more than 1300 mJ/m2 the energy distribution at the GB is non-uniform. The atom on site B has the largest energy of −3.85 eV, while the atom on site C has less, which is nearly equal to the bulk value. As a result, GB's influence on binding energies along this particular [111] line can be almost negligible, as seen in the blue circle line in Fig. 5(a). Moreover, according to Ref. [14], Σ3<110>{111} GB in bcc Fe has free volume as high as 0.31 Å (0.80 Å in our MS calculation), higher than the other three commonly-seen high-angle STGBs investigated by Ref. [21] (Σ3{112}, Σ11{332}, andΣ9{221}). High free volume at GB leads to larger tensile stress [15], which is readily seen in Fig. 5(c). Both atoms on site C and A are under tensile stress environment, with a value nearly 140% of the compressive stress of atom on site B. In nanolayered structure, since site A and C are both on the same [111] line, the local tensile stress is enhanced. This stress environment implies that the local material density is low along the [111] line, where vacancy does not prefer to stay.

In Fig. 6(a), barriers of SIA emissions and vacancy hops are plotted for a clear comparison. It is shown that in nanolayered structure the barriers are higher by an average of 13% for vacancy hopping and 14% for SIA emission. It means that nanolayered structure does not enhance these two defect absorption mechanisms. For SIA emission mechanism, which is closely related to the local stress field [10], the larger barriers due to nanolayered structure can be explained by the local tension stress near Σ3(111) STGB along that particular [111] line. But, it is noteworthy that, our observation does not indicate that the high density of Σ3(111) STGBs leads to low radiation damage tolerance. However, its high free volume offered by structural units might make such nanolayered structure a more functional sink for SIAs. Therefore more trapped SIAs after a displacement cascade in nanolayered structure are able to annihilate more vacancies by the emission mechanisms.

The competitive mechanism between conventional vacancy diffusion and SIA emission defines a spatial character of defect-GB interaction, the GB influence range. It could be concluded by comparing to the dash orange line, that the rise of hop barriers is caused only by the interstitial atom trapped in GB. This rising trend reveals a GB influence range of about 24 Å according to conventional definition (12 Å on each side of the GB). By considering a system temperature of 300° C (573.15 K), the GB influence range could be extended further to 30 Å by SIA emission mechanism at long time scale (15 Å on each side of the GB). The annihilation region in Fig. 6(a) is not precisely defined, nevertheless the "spontaneous annihilation region" with the same definition in Ref. [20] still seems to apply in our simulations.

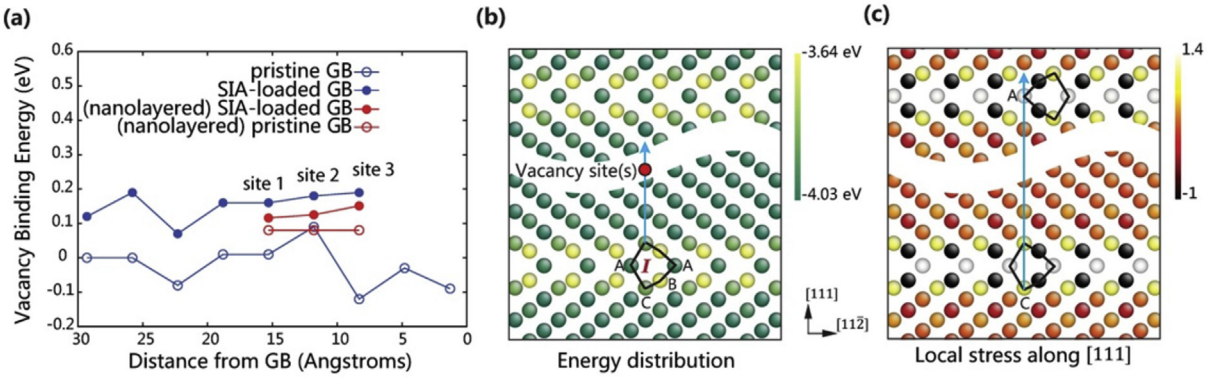

Fig. 5. (a) Binding energy of vacancies. (b) and (c), energy and local stress distribution at the structural unit of pristine GBs. In (c), stresses in the scale bar are normalized.

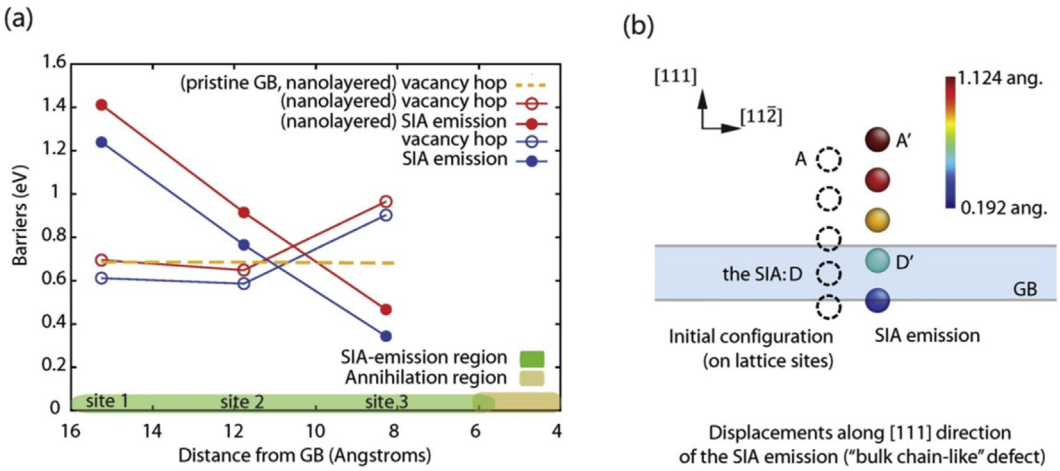

Fig. 6. (a) Barriers of SIA emission and vacancy hop as a function of distance from GB. (b) Displacements of SIA emission.

More importantly, the linear increase of the SIA emission barriers as a function of distance from GB is observed in Fig. 6(a). The calculated slope is 0.1289 eV/angstrom. Therefore SIA barrier could be expressed by

$$E^{\mathrm{SIA}}_{\mathrm{emission}} = 0.1289{*}d + K, \tag{3}$$

where d is the distance from GB, K is a constant which should be stress-environment dependent and related to the geometric and energetic character of the interstitial-loaded GB. Here for our one-GB model, K is −0.76 eV. Following this equation, we can calculate the energy barrier of BC defects in Ref. [10]. In that work, a different STGB in Fe which is also interstitial-loaded was studied. The GB induces BC ("bulk chain-like") defect into point-defect recombination process. Among the BC defects, some are "transportation type" while others are "annihilation type". Here we only focus on the "annihilation type" since it is a similar situation to what we observed in ABC sampling. Roughly the length of "annihilation type" BC defect is 12 Å. Therefore its barrier based on our equation should be 0.79 eV. This is quite consistent with their result of 0.7 eV.

We also find that the "annihilation type" BC defect in Ref. [10] is actually the same mechanism as the "interstitial emission" reported in Ref. [9], and also seen in our simulation. The first proof is the consistency on energy barrier demonstrated above. The second proof is based on geometry analysis. By comparing the descriptions of the BC defect [10] with the SIA emission [9], we notice the common point: when annihilation starts, atom movements occur simultaneously along the chain. The displacement needed for "chain-like" defect is distributed to all atoms at the same time, not like the crowdion which displaces the neighboring atoms one after another, nor like the vacancy hop which introduces individual movements equal to the neighbor distance. This phenomenon of simultaneous atom movements is also observed in our simulation, illustrated in Fig. 5(b). In this figure, the atom locations on the "chain" when SIA is emitted are shown. The atoms are separately colored by their individual displacements. It could be seen that the SIA (atom D) deviates from its original interstitial site at the GB, and atom A moves to position A′ by 1.124 Å. The displacement of atom A is approximately equals to half of the neighbor distance along <111> direction in bcc lattice, so A′ is the split interstitial site. If we look at a longer "chain", more atoms would have their locations on interstitial sites, thus satisfying the "linked interstitial–vacancy pairs" description of "annihilation type" BC defect. Therefore, the "chain" sampled by ABC method is identified to be composed of interstitial–vacancy pairs, just as BC defects. In Fe, "linked interstitial–vacancy pairs" is easy to form due to more potential interstitial sites along various directions in bcc lattice. While in Cu, because there is no stable interstitial site along <110> directions in fcc lattice, atoms do not form "linked interstitial–vacancy pairs" in SIA emission, instead, they "move about one nearest neighbor distance" [9]. Therefore, the discrepancy in geometric descriptions of these two GB-induced recombinations [9,10] is caused by the different lattice structures (fcc in Cu, bcc in Fe). Actually, they are the same mechanism in that the excess energy at the GB due to trapped SIAs is released by pushing atoms away from the GB to annihilate the vacancies nearby.

3.4. Comparing with other common GBs in alpha-Fe

In this section, we check the SIA emission barriers of other three commonly-reported high-angle STGBs, Σ9{221}, Σ11{332} and Σ3{112}, in order to demonstrate the high capability of Σ3<110>{111} GB to promote point-defect annihilation. As Fig. 7 shows, Σ9{221} GB and Σ11{332} GB are composed of structural units labeled as C and A' [21]. Similarly, there is an interstitial site in the structural unit C. Vacancies nearby could be annihilated by the interstitial atom emitted from this site. But at Σ3{112} GB, the structural unit B does not have so much free volume. Therefore a single-interstitial atom is not stable in the vicinity of the interface. Instead, two SIAs form a cluster bonded to the GB, which is not in the most common configuration of two parallel <110> dumbbells. In this work, we choose a four-SIA cluster since it has a regular configuration along the interface as the four yellow balls in Fig. 7(c) shows, and it is quite stable against dissociation.

The SIA emission barriers of different GBs as a function of the distance are plotted in Fig. 8. For {332} GB, beyond 10 Å there is no emission mechanisms found by ABC method. The one exists at 8.9 Å requires energy of 1.65 eV. While for {221} GB, SIA emissions have acceptable barriers which are slightly larger than {111} GB, along with a higher increase trend. The large energy barrier difference between {332} GB and {221} GB reveals the sensitivity of SIA emission mechanism to the interface configurations. Even though these two GBs are composed of structural units C and A′, the additional A′ between unit C at {221} GB makes the potential interstitial sites more widely separated than they are at {332} GB. Hence the emission paths along close-packed directions are also less rugged. Therefore, an interstitial atom is more easily to be pushed out of the unit C at {221} GB. Notably, the interaction

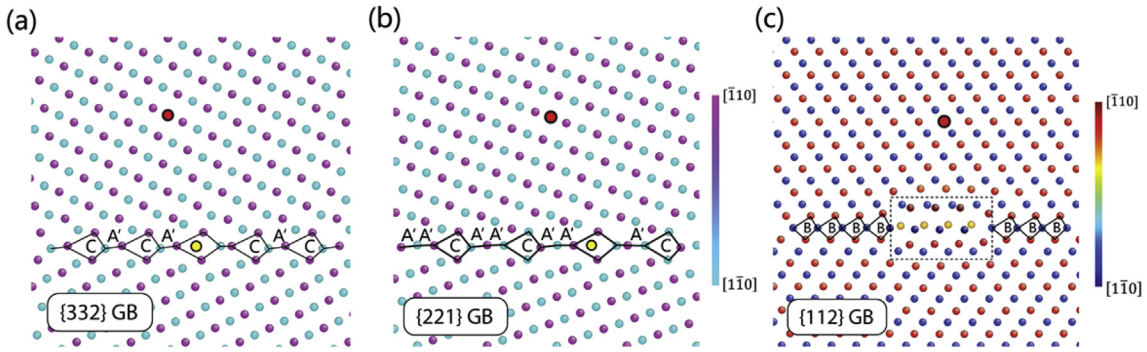

Fig. 7. The atomic configurations as initial states in the one-GB model of three other STGBs: (a) Σ9{332} GB, (b) Σ11{221} GB, and (c)Σ3{332} GB. The yellow ball represents SIA, and the large red ball represents the vacancy. (For interpretation of the references to color in this figure legend, the reader is referred to the web version of this article.)

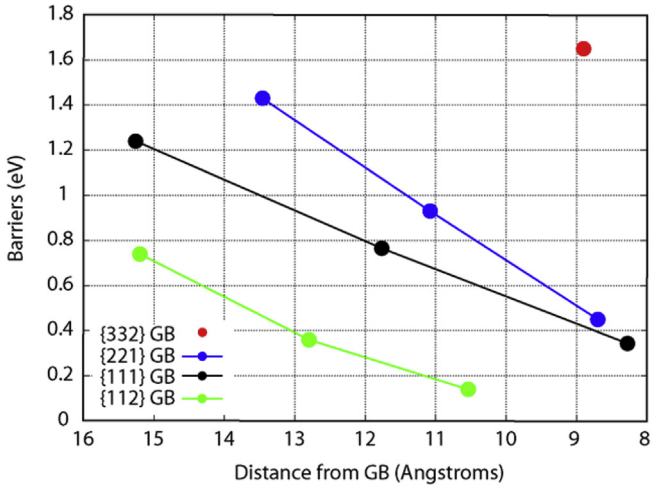

Fig. 8. Energy barriers of SIA emission for {332} GB, {221} GB, and single-interstitial atom dissociation energy for {112} GB. They are all compared with the {111} GB results in the black line.

between 4-SIA cluster and a vacancy in the vicinity of the {112} GB shows much lower energy barriers, even lower than the {111} GB. But strictly speaking, these barriers do not represent emission mechanisms. They are more likely the energies reduced by the GB for an interstitial atom dissociated from the cluster. The {112} GB is incapable of trapping any single-interstitial atom. Instead, SIAs group into a cluster by themselves, which allows off-lattice-site atoms to interact with nearby vacancies. Still, {112} GB does not always recover to its pristine form in our calculations since the SIA cluster might break down and the SIAs left at the interface lose their stability. Specifically how {112} GB is involved in this dissociation process is important, but not the interest of this article. Investigations in the future will look deeper into it. As a conclusion, among the commonly-reported high-angle STGBs, {111} GB is the ideal one for SIA emission mechanism for its capacity of trapping and emitting single-interstitial atom with lower energy barriers.

Overall, as an efficient recombination mechanism, SIA emission is more effective for self-healing of radiation damage than vacancy diffusion in the vicinity of GB. In nanolayered Fe, the effectiveness of GB to act as source for emission is suppressed by the complex local energy/stress distribution at structural units, and also by the high free volume in Σ3<110>{111} GB. Nevertheless, SIA emission is still the dominating annihilation mechanism over vacancy hopping with acceptable activation temperature at long time scale, and Σ3<110>{111} GB is the most favorable one among the four commonly-reported STGBs in alpha-Fe that enables such emission mechanisms with acceptable energy barriers.

4. Conclusions

This research investigated the potential energy landscape of SIA emission process induced by Σ3<110>{111} GB in alpha-Iron, and revealed its competition to conventional vacancy hopping mechanism. The investigation also showed how these two annihilation mechanisms are influenced by the higher GB density in nanolayered structure. Autonomous basin climbing (ABC) method was used to search potential energy surface, and to sample the atomic configurations involved in SIA emission process. Nudged elastic band (NEB) method was employed to find accurate activation energy barriers. Rate theory was applied to evaluate the activation temperature to demonstrate the extension of GB influence range at long time scale. The present results provide detailed information about the interaction between a vacancy and single-interstitial-loaded STGB in alpha-Fe. The following conclusions can be drawn from this work.

1. The SIA emission process induced by Σ3<110>{111} GB is composed of three steps (C2–C4). The evolution of energy and atomic trajectories are sampled by using the ABC method. The activation barriers are found to be in the range from 0.3 eV to 1.2 eV, which are closely related to the length of the BC defect formed in the second step of the emission process. An equation with particular constant K is established for describing the linear increase of SIA emission barrier, as a function of vacancy distance from GB.
2. It is suggested that the annihilation type of “bulk chain-like” (BC) defect discovered in bcc Fe [10] and the “interstitial emission” reported in fcc Cu [9] are the same recombination mechanism for GB-defect interactions. This conclusion is based on the energy and geometry analysis of the SIA emission found in this work. The difference of lattice structure leads to different geometric performance of GB-induced recombination mechanisms. Moreover, consistency in the energy barrier values implies that the intermediate configuration 2 (C2 in Fig. 2(a)) in our SIA emission process is the BC defect defined in previous work [10].
3. The competition between the conventional vacancy diffusion mechanism and SIA emission is examined by a comparison of energy barriers. The SIA trapped in a structural unit of GB significantly raises the vacancy hopping barrier, while greatly reduces the SIA emission barriers. Therefore the conventional GB influence range is extended by the SIA emission, which

becomes the dominant mechanism in the vicinity of the GB since it is active under certain temperatures.

4. When the GB density is high (as in nanolayered structure), both vacancy hopping and SIA emission are suppressed by the complex local energy/stress distribution at structural units of the Σ3<110>{111} STGB (induced by high free volume in the GB). The suppression is reflected by the changes of binding energy and activation barrier. This phenomenon reveals that, for certain type of STGB, more stable interstitial sites at interface and enhanced self-healing property cannot be obtained together. But comparing with three other commonly-reported STGBs in alpha-Fe, it is still reasonable to construct nanolayered material using {111} GB, for it is indeed potentially a better sink for SIAs and benefits SIA emission as well.

Acknowledgments

This work was supported by Chinese Nature Science Foundation (11372032). XZT sincerely appreciate the hospitality of the Nuclear Science and Engineering Department at MIT for an academic visit. YF thanks the support of Eugene P. Wigner Fellowship at the Oak Ridge National Laboratory, managed by UT-Battelle, LLC, for the U.S. Department of Energy (No. DEAC05-00OR22725). Authors would like to express their great gratitude to Lixin Sun at MIT for lots of helpful discussions. Particularly, the results addressed in this paper have been achieved using the codes written by Lixin Sun, which realizes ABC implementation in LAMMPS.

References

[1] I. Chant, K.L. Murty, Structural materials issues for the next generation fission reactors, JOM 62 (2010) 67–74.
[2] P. Yvon, F. Carré, Structural materials challenges for advanced reactor systems, J. Nucl. Mater. 385 (2009) 217–222.
[3] L. Yang, F. Gao, R.J. Kurtz, X.T. Zu, S.M. Peng, X.G. Long, X.S. Zhou, Effects of local structure on helium bubble growth in bulk and at grain boundaries of bcc iron: A molecular dynamics study, Acta Mater. 97 (2015) 86–93.
[4] N. Nita, R. Schaeublin, M. Victoria, Impact of irradiation on the microstructure of nanocrystalline materials, J. Nucl. Mater. 329–333 (Part B) (2004) 953–957.
[5] Y. Osetsky, N. Anento, A. Serra, D. Terentyev, The role of nickel in radiation damage of ferritic alloys, Acta Mater. 84 (2015) 368–374.
[6] M.J. Demkowicz, R.G. Hoagland, J.P. Hirth, Interface structure and radiation damage resistance in Cu-Nb multilayer nanocomposites, Phys. Rev. Lett. 100 (2008) 136102.
[7] E.G. Fu, A. Misra, H. Wang, L. Shao, X. Zhang, Interface enabled defects reduction in helium ion irradiated Cu/V nanolayers, J. Nucl. Mater. 407 (2010) 178–188.
[8] X.-M. Bai, B. Uberuaga, The influence of grain boundaries on radiation-induced point defect production in materials: a review of atomistic studies, JOM 65 (2013) 360–373.
[9] X.-M. Bai, A.F. Voter, R.G. Hoagland, M. Nastasi, B.P. Uberuaga, Efficient annealing of radiation damage near grain boundaries via interstitial emission, Science 327 (2010) 1631–1634.
[10] C. Di, J. Wang, T. Chen, L. Shao, Defect annihilation at grain boundaries in alpha-Fe, Sci. Rep. 3 (2013).
[11] A. Kushima, X. Lin, J. Li, J. Eapen, J.C. Mauro, X. Qian, P. Diep, S. Yip, Computing the viscosity of supercooled liquids, J. Chem. Phys. 130 (2009) 224504.
[12] T. Jourdan, J.-P. Crocombette, Rate theory cluster dynamics simulations including spatial correlations within displacement cascades, Phys. Rev. B 86 (2012) 53–58.
[13] G.J. Ackland, M.I. Mendelev, D.J. Srolovitz, S. Han, A.V. Barashev, Development of an interatomic potential for phosphorus impurities in alpha-iron, J. Phys.-Condens. Mater. 16 (2004) S2629–S2642.
[14] S.K. Bhattacharya, S. Tanaka, Y. Shiihara, M. Kohyama, Ab initio perspective of the <110> symmetrical tilt grain boundaries in bcc Fe: application of local energy and local stress, J. Mater. Sci. 49 (2014) 3980–3995.
[15] S.K. Bhattacharya, S. Tanaka, Y. Shiihara, M. Kohyama, Ab initio study of symmetrical tilt grain boundaries in bcc Fe: structural units, magnetic moments, interfacial bonding, local energy and local stress, J. Phys.-Condens. Mater. 25 (2013) 1798–1801.
[16] J.D. Rittner, D.N. Seidman, <110> symmetric tilt grain-boundary structures in fcc metals with low stacking-fault energies, Phys. Rev. B (1996) 6999–7015.
[17] L.S. Shvindlerman, G. Gottstein, V.A. Ivanov, D.A. Molodov, D. Kolesnikov, W. Łojkowski, Grain boundary excess free volume-direct thermodynamic measurement, J. Mater. Sci. 41 (2006) 7725–7729.
[18] M.A. Tschopp, G.J. Tucker, D.L. McDowell, Structure and free volume of <110> symmetric tilt grain boundaries with the E structural unit, Acta Mater. 55 (2007) 3959–3969.
[19] M.R. Sørensen, Y. Mishin, A.F. Voter, Diffusion mechanisms in Cu grain boundaries, Phys. Rev. B 62 (2000) 3658.
[20] X. Li, W. Liu, Y. Xu, C.S. Liu, Q.F. Fang, B.C. Pan, J.-L. Chen, G.-N. Luo, Z. Wang, Principal physical parameters characterizing the interactions between irradiation-induced point defects and several tilt symmetric grain boundaries in Fe, Mo and W, J. Nucl. Mater. 444 (2014) 229–236.
[21] F. Gao, X. Sun, M.A. Khaleel, M.A. Tschopp, K.N. Solanki, M.F. Horstemeyer, Probing grain boundary sink strength at the nanoscale: energetics and length scales of vacancy and interstitial absorption by grain boundaries in alpha-Fe, Phys. Rev. B 85 (2012).
[22] H.L. Heinisch, F. Gao, R.J. Kurtz, The effects of interfaces on radiation damage production in layered metal composites, J. Nucl. Mater. 329-333 (2004) 924–928.
[23] A. Misra, M.J. Demkowicz, X. Zhang, R.G. Hoagland, The radiation damage tolerance of ultra-high strength nanolayered composites, JOM 59 (2007) 62–65.
[24] J. Wang, R.G. Hoagland, J.P. Hirth, A. Misra, Atomistic simulations of the shear strength and sliding mechanisms of copper-niobium interfaces, Acta Mater. 56 (2008) 3109–3119.
[25] E.G. Fu, A. Misra, H. Wang, L. Shao, X. Zhang, Interface enabled defects reduction in helium ion irradiated Cu/V nanolayers, J. Nucl. Mater. 407 (2010) 178–188.
[26] S. Plimpton, Fast parallel algorithms for short-range molecular dynamics, J. Comput. Phys. 117 (1995) 1–19 http://dx.doi.org/10.1006/jcph.1995.1039.
[27] Y. Fan, A. Kushima, B. Yildiz, Unfaulting mechanism of trapped self-interstitial atom clusters in bcc Fe: a kinetic study based on the potential energy landscape, Phys. Rev. B 81 (2010).
[28] Y. Fan, A. Kushima, S. Yip, B. Yildiz, Mechanism of void nucleation and growth in bcc Fe: atomistic simulations at experimental time scales, Phys. Rev. Lett. 106 (2011) 125501.
[29] T.T. Lau, A. Kushima, S. Yip, Atomistic simulation of creep in a nanocrystal, Phys. Rev. Lett. 104 (2010) 175501 http://dx.doi.org/10.1103/PhysRevLett.104.175501.
[30] M. Rajagopalan, M.A. Tschopp, K.N. Solanki, Grain boundary segregation of interstitial and substitutional impurity atoms in alpha-iron, JOM 66 (2014) 129–138.
[31] J. Li, AtomEye: an efficient atomistic configuration viewer, Model. Simul. Mater. Sci. Eng. 11 (2003) 173.